Electronic Supplementary Information

Catalytic Hydrogenation of CO_2 by Unsymmetric N-Heterocyclic Carbene-Nitrogen-Phosphine Ruthenium Complexes

Li Ji,‡ Tianhua Cui,‡ Xufeng Nie, Yanling Zheng, Xueli Zheng, Haiyan Fu, Maolin Yuan, Hua Chen, Jiaqi Xu,* and Ruixiang Li*

Key Laboratory of Green Chemistry and Technology of Ministry of Education, College of Chemistry, Sichuan University, Chengdu, Sichuan 610064, China

E-mail: jqxu@scu.edu.cn
liruixiang@scu.edu.cn

‡ These authors contributed equally to this work.

General: Unless otherwise noted, the manipulations, which are sensitive to moisture or air, were performed in an argon-filled glove box VIGOR or treated by standard Schlenk techniques. NMR spectra were recorded on a Bruker AVII-400 spectrometer at 400 MHz (^{1}H NMR), and 162 MHz (^{31}P NMR). Chemical shifts were reported in ppm down field from internal Me_4Si and external 85% H_3PO_4, respectively.

All the solvents used for reactions were distilled under argon after drying over an appropriate drying agent. All other commercially available reagents were purchased from Aladdin, Adamas, Aldrich and Alfa Aesar Chemical Company.

We thank Comprehensive Training Platform of the Specialized Laboratory in the College of Chemistry at Sichuan University and Analytical & Testing Center of Sichuan University for the support. We would like to thank Dr. Daibing Luo and Dr. Daichuan Ma from the Analytical & Testing Center of Sichuan University for X-ray diffraction work and single crystal analysis. We thank Ms. Yue Qi of the comprehensive training platform of the Specialized Laboratory in the College of Chemistry at Sichuan University for compound testing.

Preparation of Ligands and Ru Complexes:

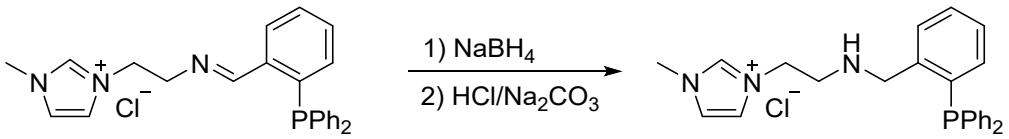

L1 **L2**

Scheme S1. Synthesis of 3-(2-{[2-(diphenylphosphino)benzyl]amino}ethyl)-1-methyl-1H-imidazol-3-ium chloride [CN(H)P] ligand (**L2** ligand).

L1 ligand 3-(2-{[2-(diphenylphosphino)benzylidene]amino}ethyl)-1-methyl-1*H*-imidazol-3-ium chloride was prepared according to the previous literature.[1] 1.5 eq of $NaBH_4$ (285 mg, 7.5 mmol) was slowly added into the MeOH solution of 3-(2-{[2-(diphenylphosphino)benzylidene]amino}ethyl)-1-methyl-1*H*-imidazol-3-ium chloride **L1** ligand (1.985 g, 5 mmol) in ice bath and stirred at room temperature for 3 h . After the reaction, the solution with excessive $NaBH_4$ was quenched with dilute hydrochloric acid, followed by 2 eq $NaHCO_3$ to neutralize the solution. The aqueous solution was extracted with CH_2Cl_2 (3×15 ml). The organic phase was separated, dried with Na_2SO_4 and filtered. At last, the filtrate was evaporated under vacuum to afford a pale yellow viscous liquid (1.59 g, yield 80%).

^{1}H NMR (400 MHz, DMSO-d_6) δ (ppm) 9.23 (s, 1H), 7.77-7.64 (m, 2H), 7.40 (dq, J = 3.2, 1.4 Hz, 7H), 6.76 (ddd, J = 7.7, 4.4, 1.3 Hz, 1H), 4.17 (t, J = 5.6 Hz, 2H), 3.86 (s, 3H), 3.83 (d, J = 2.2 Hz, 2H), 2.80 (t, J = 5.7 Hz, 2H). ^{31}P NMR (DMSO-d_6, 162.0 MHz) δ (ppm) -17.1.

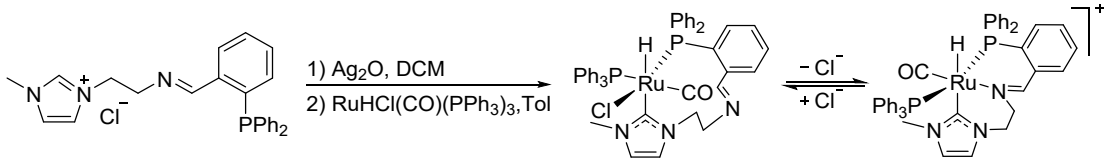

Scheme S2. Synthesis of CNP ligand chelated complex **1**.[2]

Ru-CNP complex **1** were prepared according to the previous literature.[1] The mixture of ligand **L1** and Ag_2O in dichloromethane was stirred at room temperature for 2 h, and then the dichloromethane solution was filtered. The filtrate was added to anhydrous diethyl ether to precipitate Ag complex. Subsequently, the silver complex reacted with $RuHCl(CO)(PPh_3)_3$ in toluene at 60 °C to form the desired product as a pale yellow powder in 71% yield. The pure complex **1a** could be isolated by column chromatography, while complex **1b** was obtained by refluxing in THF and purified by column chromatography. However, when pure complex **1a** (or **1b)** was dissolved in the solution, it would transform into complex **1b** (or **1a**) and reach the equilibrium (Figure S13-14).

^{1}H NMR (DMSO-d_6, 400.1 MHz, δ): 8.64 (s), 8.63 (s), 7.83 (m), 7.49 (m), 6.8− 7.4 (m), 6.77−7.64 (m), 6.58 (s), 6.45 (t), 6.20 (t), 4.39−4.52 (m), 4.02 (d), 3.99 (d, 1H, J = 16.0 Hz), 3.89 (s), 3.61 (d), 3.47 (t), 2.96 (s), 2.59 (t), 2.31 (t), −7.53 (dd), −11.96 (dd). ^{31}P NMR (DMSO- d_6, 162.0 MHz, δ): 47.4 (d, JP-P = 256.5 Hz), 41.3 (dd, JP-P = 30.4 Hz), 42.5 (d, JP-P = 256.5 Hz), 36.4 (dd, JP-P = 30.4 Hz) .

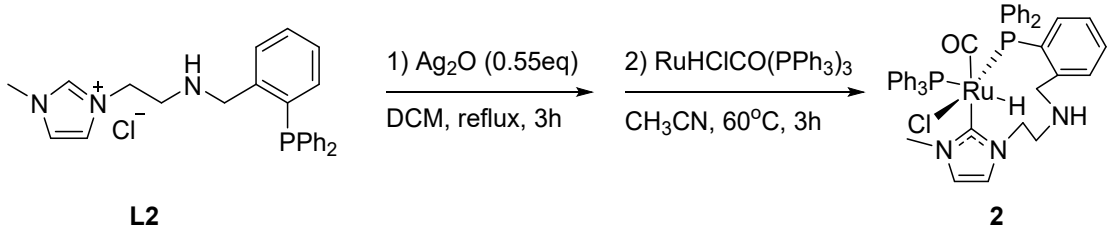

Scheme S3. Synthesis of CN(H)P ligand chelated complex **2**.

L2 ligand (870.2 mg, 2 mmol), silver oxide (255.2 mg, 1.1 mmol) and DCM (10 mL) were successively added into a 50 mL two-necked flask under the protection of nitrogen, and the reaction was stopped after being stirred in the reflux for 2 h without light. The insoluble matter was filtered to obtain a brown clear solution. Then 30 mL anhydrous diethyl ether was added and the white solid was precipitated out. The mother liquor was filtered out, and the solid was washed with ether for three times (10 ml×3), and the product **L2-Ag** was dried in vacuum (0.890g yield, 82% yield).

L2-Ag complex (54.1 mg, 0.1 mmol) and ruthenium precursor $RuHCl(CO)(PPh_3)_3$ (95.1 mg, 0.1 mmol) were added to a 50 mL dry two-necked flask under the protection of nitrogen, followed by acetonitrile (8 mL) and stirred at 60 °C for 3 h. Then the solution was cooled to room temperature, the insoluble matter was filtered out. The filtrate was drained under reduced pressure, the obtained solid was dissolved with 5ml DCM, and then precipitated with 20ml n-hexane. The crude product was eluted by

neutral Al_2O_3 column chromatography with a 10:1 eluent of CH_2Cl_2: CH_3OH, and the yield of complex **2** was 27.7 mg (35% yield).

^1H NMR (400 MHz, DMSO-d6) δ (ppm) 7.78-7.51 (m, 12H), 7.49-7.37 (m, 19H), 7.35-7.26 (m, 17H), 7.16 (dt, J = 4.4, 2.8 Hz, 4H), 6.95 (t, J = 8.0 Hz, 1H), 6.46 (t, J = 8.8 Hz, 2H), 4.22 (t, J = 6.6 Hz, 2H), 3.85-3.78 (m, 2H), 2.99 (s, 2H), 2.81 (s, 3H), -6.94 (dd, J = 97.2, 28.7 Hz, 1H). ^{31}P NMR (162 MHz, DMSO-d6) δ (ppm) 44.89 (d, J = 15.1 Hz), 17.97. HRMS (ESI-TOF) m/z: $[M-Cl]^+$ Calcd for $C_{44}H_{42}N_3OP_2Ru$: 792.1841, found: 792.1848.

Catalytic hydrogenation of CO_2 with H_2:

Catalytic CO_2 hydrogenation was carried out in a Hastelloy Autoclave Reactor system equipped with a 25 mL cylinder. The catalyst (0.02-1 μmol) was dissolved in a degassed aqueous solution (5 mL) of CsOH (10 mmol) along with the addition of 1 ml THF. The reactor was pressurized with 5 MPa of CO_2/H_2(1:1) and heated at 100-200 °C for the appropriate time (4-96 h). 50-200 μl of dimethylformamide was added as internal standard, while 500 μl D_2O was added as the solvent. Then, the formate was quantified by ^1H NMR spectroscopy.

The conditions to test the effects of different salts (KNO_3, $NaBF_4$, NaOAc, CF_3COONa, etc.) were same to the general conditions, except that certain amount of salt (salt:cat = 20000-100000) was added.

To uncover the underlying mechanism, stoichiometric reactions were conducted with 30 μmol Ru-CNP complex **1** and 1 mmol CsOH under 5 MPa of CO_2/H_2 (CO_2 : H_2 = 1 : 1) in the mixture solvent of CD_3CN and D_2O (1.5mL: 0.5mL) at 140 °C for 2 h, in which the intermediates were monitored by in-situ NMR. In the stoichiometric reactions, the amount of Ru-CNP complex **1** was increased to enhance the possibility of capturing intermediates.

Mercury poisoning experiments:

The mercury poisoning experiments were carried out in a Hastelloy Autoclave Reactor system equipped with a 25 mL cylinder, the catalyst (0.1 μmol) was dissolved in a degassed aqueous solution (5 mL) of CsOH (10 mmol) along with the addition of 1 ml THF and 9 μl Hg. The reactor was pressurized with 5 MPa of CO_2/H_2(1:1) and heated at 140 °C for 4 h. 100 μl of dimethylformamide was added as internal standard, while 500 μl D_2O was added as the solvent. Then, the formate was quantified by ^1H NMR spectroscopy.

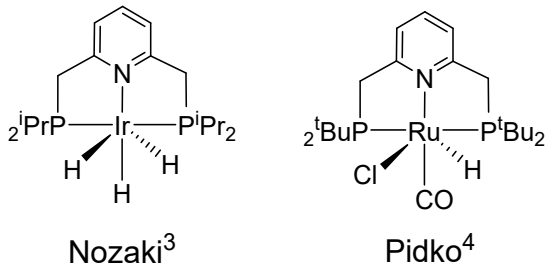

Nozaki[3] Pidko[4]

Scheme S4. Representative catalysts based on PNP ligands.[3, 4]

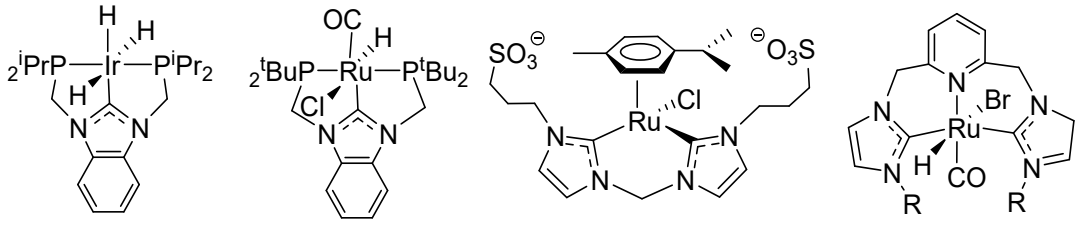

Scheme S5. Representative catalysts based on NHC ligands.[5-8]

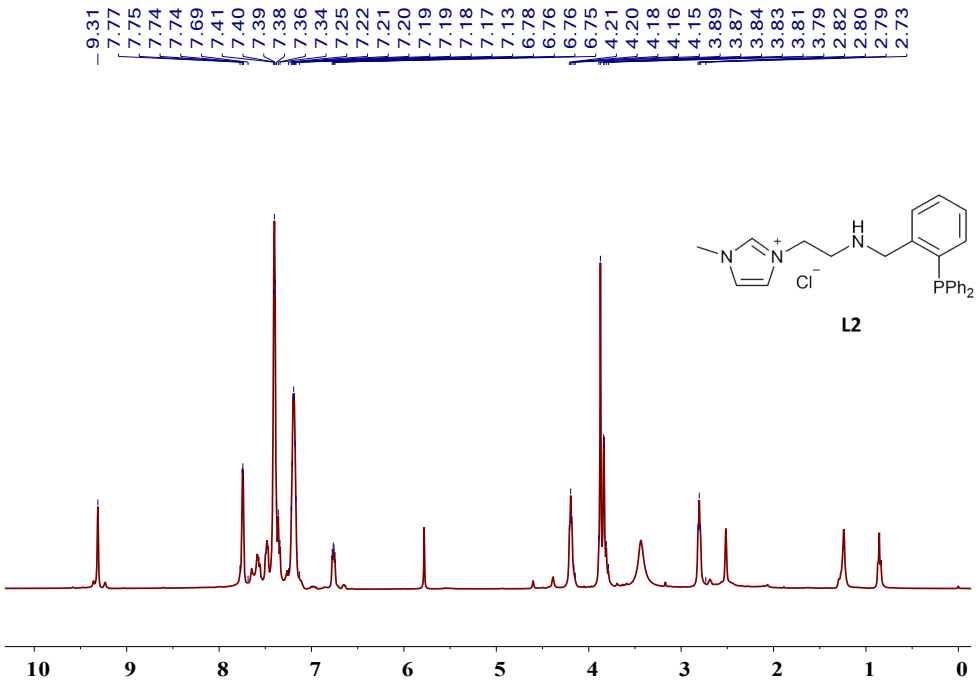

Figure S1. ^{1}H NMR spectrum of **L2** ligand (400.1 MHz, DMSO-d_6).

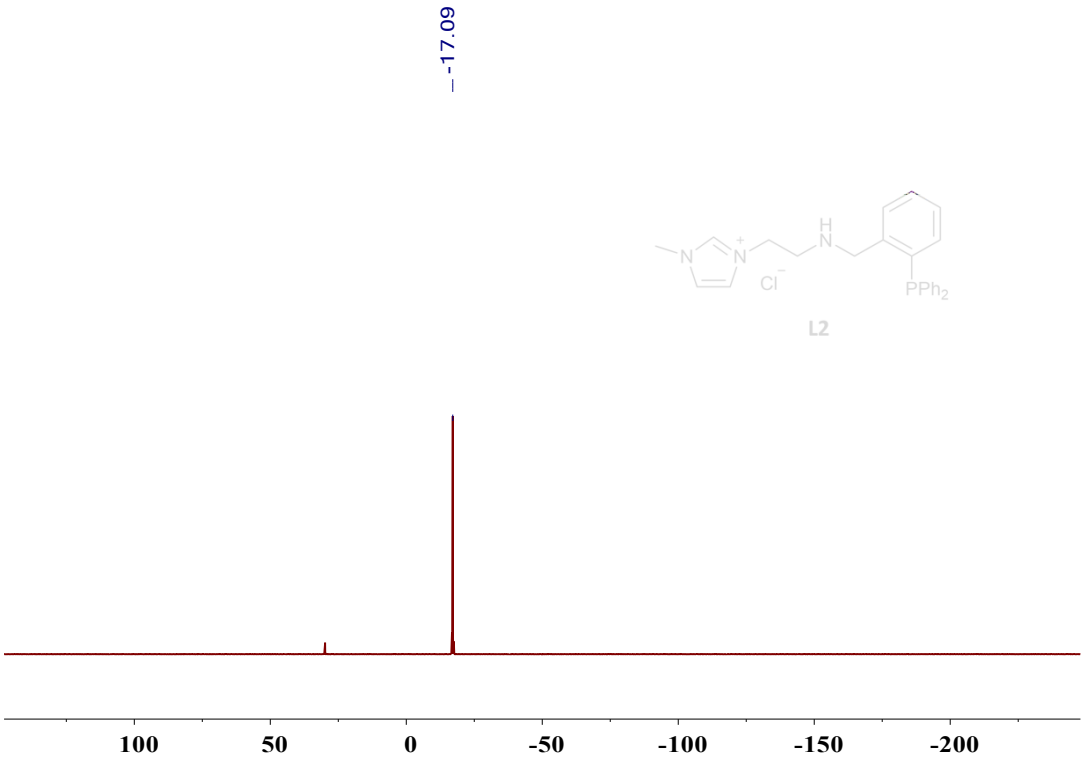

Figure S2. ^{31}P NMR spectrum of **L2** ligand (162.0 MHz, DMSO-d_6).

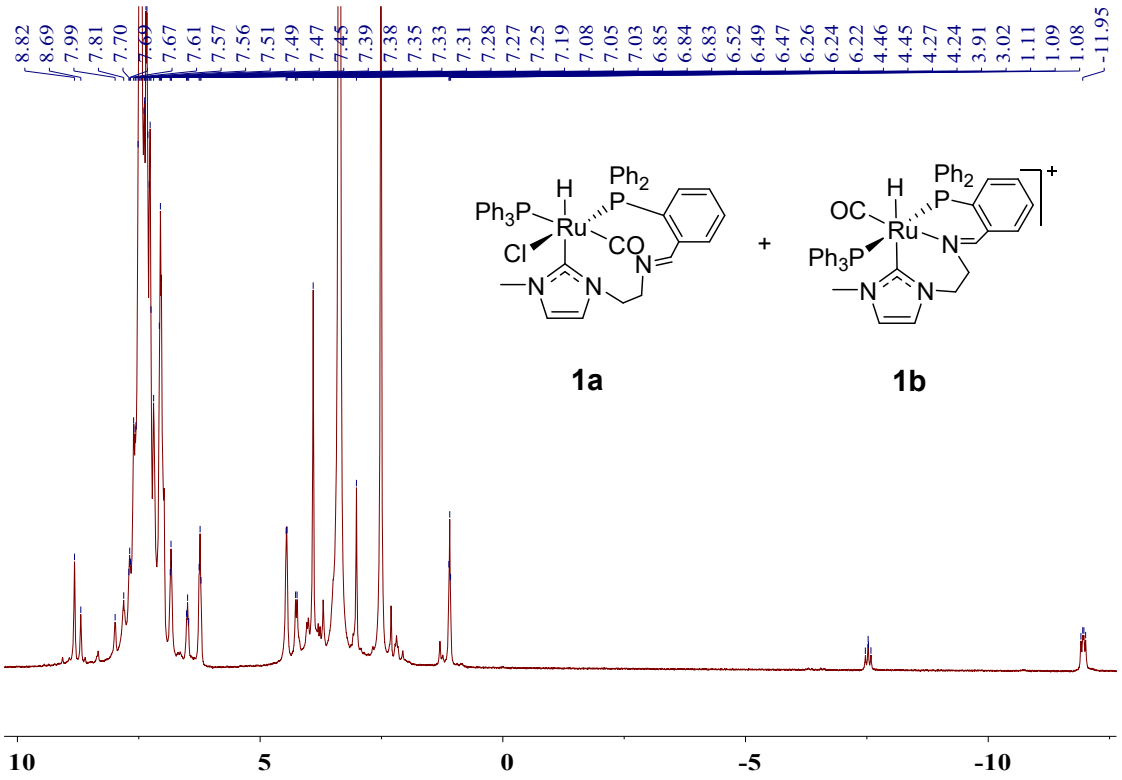

Figure S3. ^{1}H NMR spectrum of complex **1** (400.1 MHz, DMSO-d_6)**.**

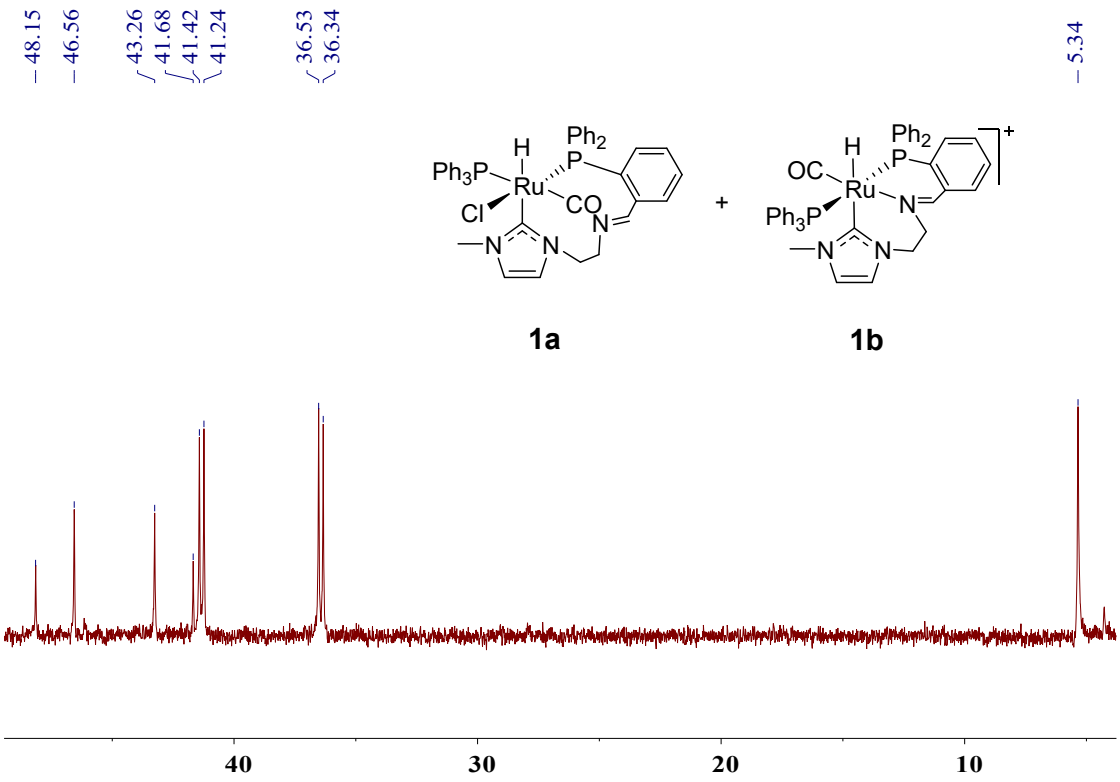

Figure S4. ^{31}P NMR spectrum of complex **1** (162.0 MHz, DMSO-d_6).

The characteristic signals of hydride in complex **1** showed two groups of peaks at −11.96 ppm (dd, J = 24.3, 14.6 Hz, 1H) and −7.53 ppm (dd, J = 24.8, 22.0 Hz, 1H) in the ^{1}H NMR spectrum (Figure S3). The ^{31}P NMR spectrum also gave two sets of doublets (Figure S4), one was located at 47.4 and 42.5 ppm (d, J = 256.5 Hz), while the other was at 41.3 and 36.4 ppm (d, J = 30.4Hz).

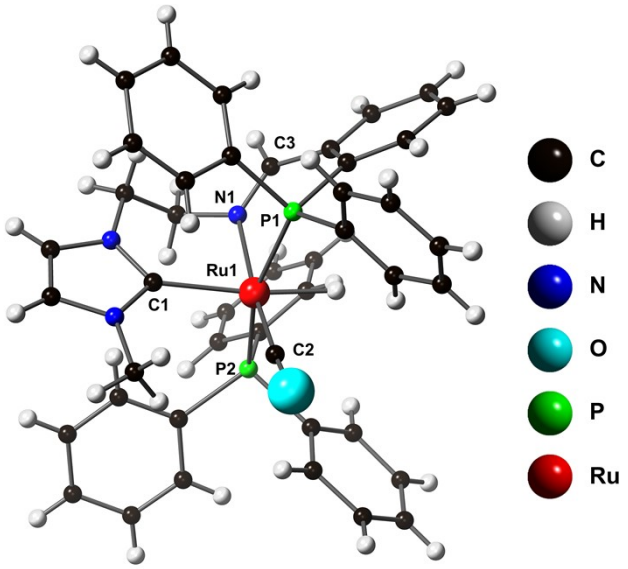

Figure S5. The single crystal structure of complex **1b** (This structure was obtained from Reference

2). Selected bond lengths (Å): Ru1-C1=2.179, Ru1-N1=2.178, Ru1-P1=2.315, Ru1-P2=2.379, Ru1-C2=1.832. Selected bond angles (°): C1-Ru1-P1=97.682, C1-Ru1-N1=84.371, N1-Ru1-P1=83.316, C3-N1-Ru1= 129.543.

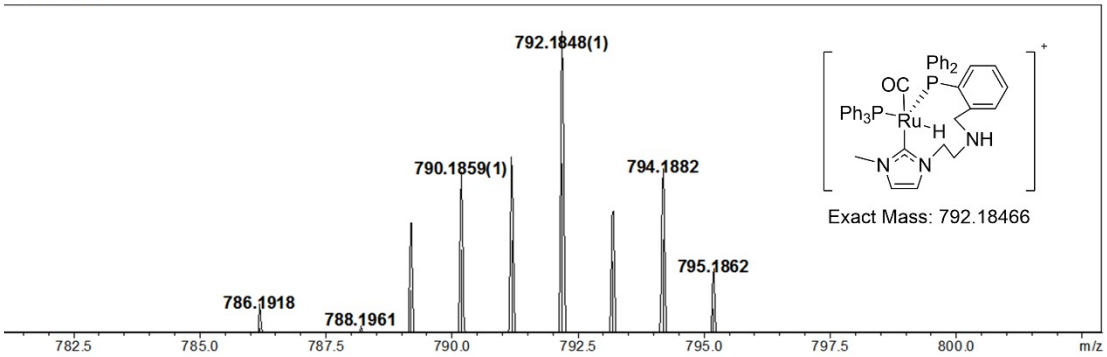

Figure S6. ESI-MS spectrum of complex **2**.

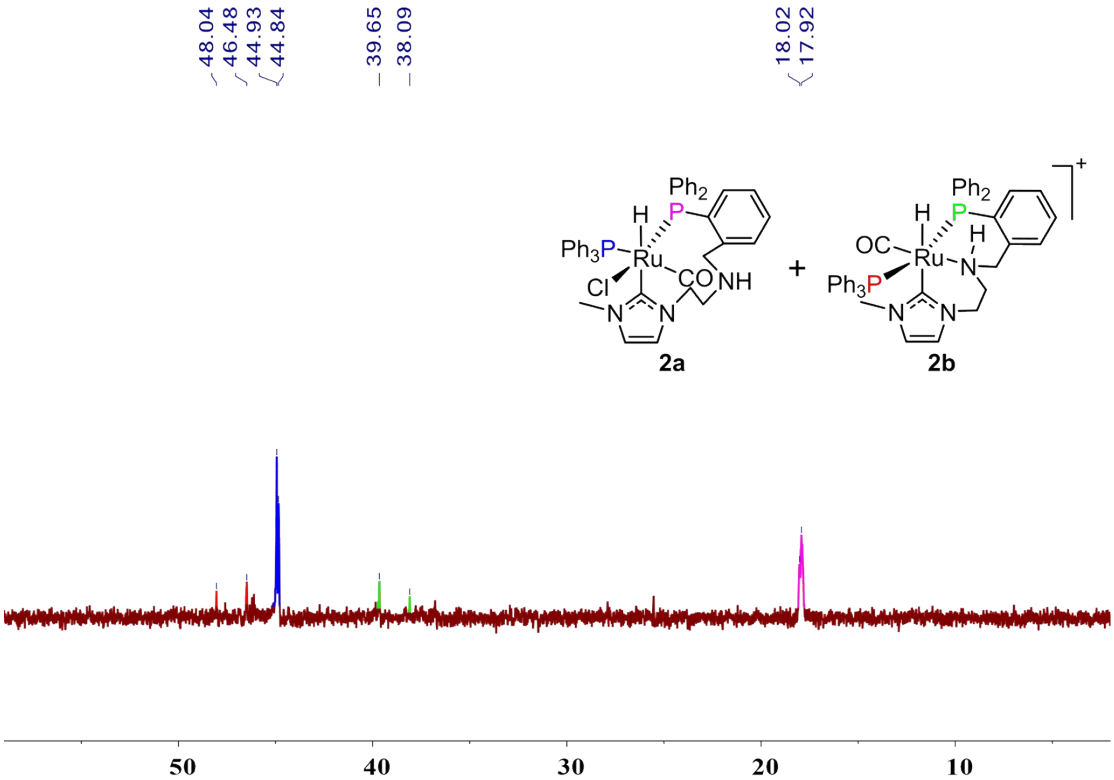

Figure S7. ^{31}P NMR spectrum of complex **2** (162.0 MHz, DMSO-d_6) (blue and purple peaks represent P in complex **2a**, red and green peaks represent P in complex **2b**).

The ^{31}P spectrum of complex **2** (Fig. N1) indicates there existed a similar equilibrium in complex **2** just like that of complex **1**. But the trend for complex **2** was significantly lower than that of complex **1.** As reveals in Fig. S5, the C3-N1-Ru1 bond angle of complex **1b** is 129°. Compared with the N atom of -CH=N- moiety in CNP ligand, the N atom of N-H moiety in Ru-CN(H)P complex **2** is sp^3 hybridization and has a smaller bond angle (around 108°). Therefore, we supposed that the N atom of N-H moiety in CN(H)P ligand was more difficult to form a coordination bond with Ru center.

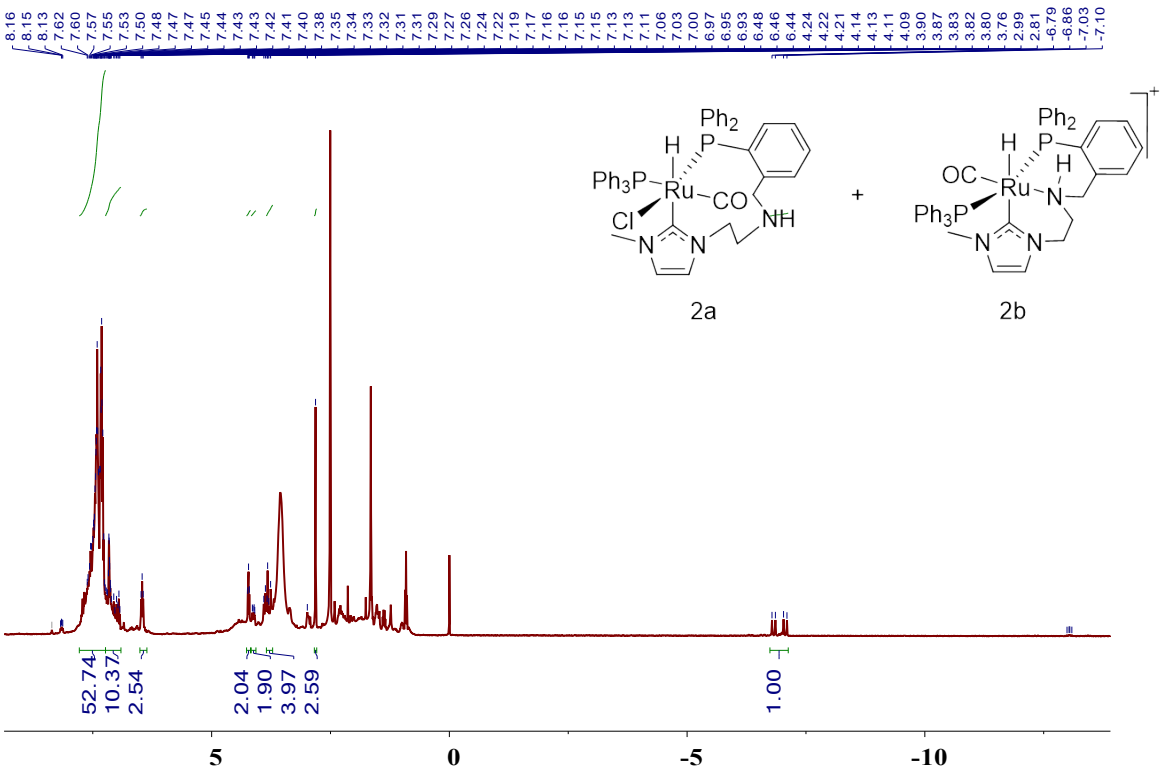

Figure S8. ^{1}H NMR spectrum of complex **2** (400.1 MHz, DMSO-d_6).

The ^{1}H NMR spectrum (Fig. S8) of the hydride in complex **2** exhibited two sets of doublet of doublets. One was located at −6.94 ppm (dd, J = 29.0 Hz), indicating that two P atom occupied in *cis*-position of the hydride. And the other was located at – 13.04 ppm (dd, J = 16.0 Hz), which indicated that the hydride was also located in the *cis*-position of two phosphorus atoms.

Table S1. Comparison of stability of representative Ru catalysts for the hydrogenation of CO_2[a].

Cat.	T (°C)	$Time_{start}$ (h)	TOF_{start} (h^{-1})	$Time_{total}$ (h)	$TOF_{average}$ (h^{-1})	TON	Ref.
1 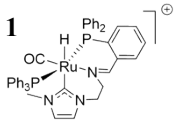	140	4	700	96	620	59500	This work
	200	4	5725	48	3520	169000	
2 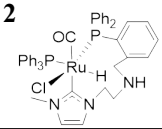	140	4	418	16	334	5340	This work
S1 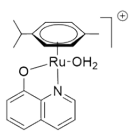	100	2	97	20	20	400	[9]
S2 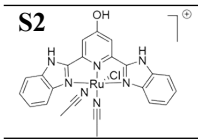	100	—	—	24	17	407	[10]

S3 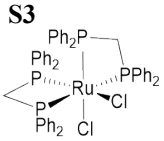	70[b]	7	420	20.75	262	4010	[11]
	70[c]	0.05	180000	0.5	35000	14540	
S4 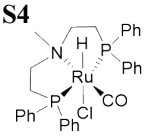	70	—	—	9.83	1096	10775	[12]
S5 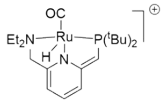	200	4	2250	48	479	23000	[13]
S6 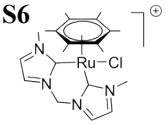	200	1	2500	75	307	23000	[14]
S7 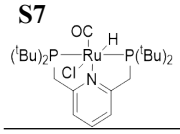	132	—	—	0.04	1892000	76000	[4]
S8 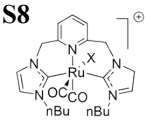	120[d]	4	20600	72	11580	833800	[15]

[a] $Time_{start}$ represents the initial reaction time, TOF_{start} represents the average value of TOF during $Time_{start}$, $Time_{total}$ represents the total reaction time, and $TOF_{average}$ represents the average value of TOF during the total reaction time; [b] in Tol; [c] in methyl isobutyl carbinol (MIBC); [d] in 1-butyl-2,3-dimethylimidazolium acetate (BMMI).

Table S2. Hydrogenation of CO_2 by complex **1** under different conditions[a].

entry	Cat. (μmol)	T (°C)	Formate		
			[μmol]	TON	TOF
1[b]	0.1	140	149	1500	375
2[b]	0.1	140	120	1200	300
3[b]	0.1	140	216	2160	540
4	0.1	100	21	206	41
5	0.1	120	43	428	107
6[c]	0.1	140	10	104	26
7[c]	0.1	140	45	448	112
8[d]	0.1	140	556	5560	695
9[d]	0.1	140	1068	10700	668
10	0.02	200	455	22800	5700
11[d]	0.02	200	3399	170000	2361

[a] General conditions: T = 140 °C, complex **1** (0.1 μmol), base (CsOH, 10 mmol), $P(H_2) = P(CO_2) =$ 2.5 MPa, $V(THF)/V(H_2O)$ (1:5, 6 ml), reaction time = 4 h; [b] base = LiOH (entry1), NaOH (entry 2), KOH (entry 3); [c] $P(CO_2) = 0$, base = Cs_2CO_3 (entry 6), $CsHCO_3$ (entry 7); [d] reaction time = 8 h

(entry 8), 16 h (entry 9), 72 h (entry 11); TOF is an average value and calculated according to the reaction time.

The effect of the various bases on the reaction were investigated (Table 1, entry 1; Table S2, entry 1-3), the results indicated the presence of base was of vital importance, the highest TOF (699 h^{-1}) was given in the presence of CsOH (Table 1, entry 1).

When H_2 was solely used with $CsHCO_3$ as the base, considerable amount of formate was observed (Table S2, entry 6). However, a negligible amount of formate was obtained when Cs_2CO_3 was used to substitute $CsHCO_3$ (Table S2, entry 7). The phenomenon was in consistent with the reported, indicating that HCO_3^- could serve as both the source of CO_2 and the base.[16]

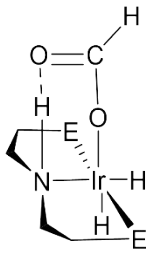

Figure S9. Six-membered ring between Ir complex and CO_2.[17]

The metal complexes with meridional configuration could easily form six-membered ring transition state with CO_2 (Fig. S9).[17]

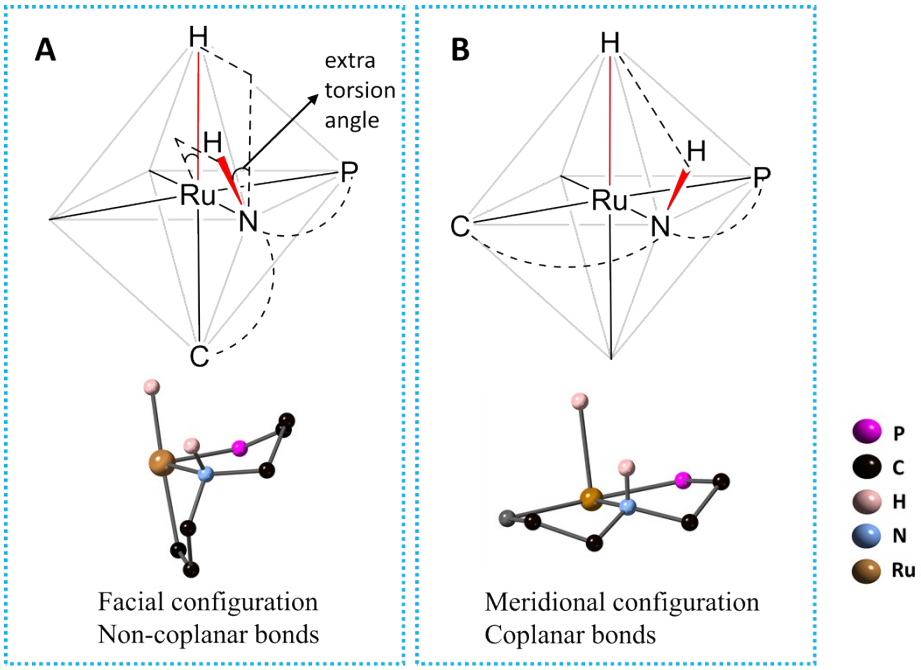

Figure S10. Schematic diagrams of the N-H bond and the Ru-H in different coordination forms. (A) Facial configuration; (B) Meridional configuration.

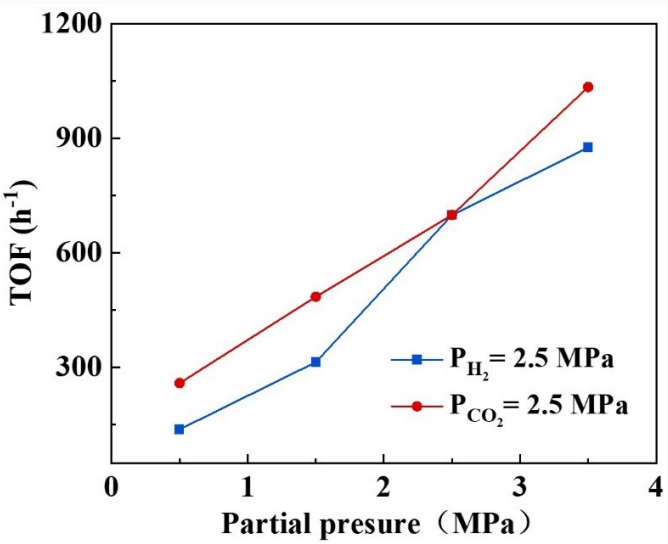

Figure S11. Pressure-dependent reaction rates[a].

[a] General conditions: T = 140 °C, complex **1** (0.1 μmol), base (CsOH, 10 mmol), P(H_2) or P(CO_2) = 2.5 MPa, V(THF)/V(H_2O) (1:5, 6 ml), reaction time = 4 h.

Table S3. CO_2 hydrogenation performance of complex **1** under different pressure or in the presence of different additive[a].

entry	Additive	H_2:CO_2(MPa)	pKa (conjugated acid)	additive:cat	TOF (h^{-1})
1	N/A	0.5:2.5	N/A	N/A	259
2	N/A	1.5:2.5	N/A	N/A	485
3	N/A	2.5:2.5	N/A	N/A	700
4	N/A	3.5:2.5	N/A	N/A	1030
5	N/A	2.5:0.5	N/A	N/A	138
6	N/A	2.5:1.5	N/A	N/A	314
7	N/A	2.5:3.5	N/A	N/A	876
8[b]	N/A	1.0:1.0	N/A	N/A	170
9	N/A	1.0:1.0	N/A	N/A	119
10	N/A	2.0:1.0	N/A	N/A	244
11	N/A	1.0:2.0	N/A	N/A	321
12	KNO_3	2.5:2.5	-1.76	50000	675
13	K_2SO_4	2.5:2.5	1.99	50000	1190
14	$NaBF_4$	2.5:2.5	0.5	50000	821
15	NaOAc	2.5:2.5	6.74	50000	1960
16	$C_6H_5CO_2Na$	2.5:2.5	4.21	50000	1690
17	CF_3COONa	2.5:2.5	0.23	50000	976
18	Hg	2.5:2.5	N/A	6000	632

[a] General conditions: Complex **1** (0.1 μmol), base = CsOH (10 mmol), V(THF)/V(H_2O) = 1:5 (6 ml), reaction time = 4 h. T = 140 °C; [b]H_2:CO_2:N_2=1.0:1.0:1.0

To see if the higher total pressure could increase the TOF, the ratio of H_2 and CO_2 was kept constant, while N_2 (inert gas) was added to increase the total pressure. As a result, the TOF for formate would increase by simply increasing the total pressure (Table S3, entry 8, 9). However, the TOF could increase much more when the total pressure was increased by increasing the partial pressure of H_2 or CO_2 (Table S3, entry 8-11). Moreover, to see the impacts of only changing the partial pressure of H_2 or CO_2 on the TOF, N_2 was added to keep the total pressure constant. The TOF would also decrease by lowering the partial pressure of H_2 or CO_2, when the total pressure was kept constant (Table S3, entry 8, 10-11). Therefore, the TOF is directly related to the total pressure, partial pressure of H_2 and CO_2.

Moreover, the experimental results showed that the addition of OAc^- could significantly increase the activity of Ru-CNP complex **1** (Table S3, entry 15).

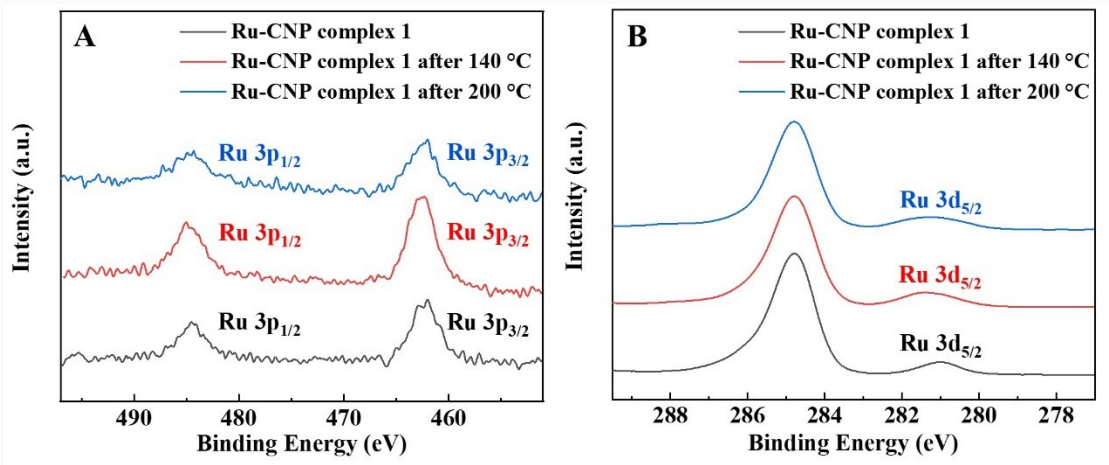

Figure S12. (A) Ru 3p and (B) Ru 3d XPS spectra of Ru-CNP complex **1** before (black) and after CO_2 hydrgogenation reaction at 140 °C (red) and 200 °C (blue) for 4 h.

We have carried out mercury poisoning experiments and XPS tests to rule out the influence of nanoparticle catalysis. If there were Ru nanoparticles during the reaction, they would form amalgam and out of action in the mercury poisoning experiments.[18] The TOF was 632 h^{-1} for Ru-CNP complex **1** in the mercury experiment (Table S3, entry18). Compared with the original value (TOF = 700 h^{-1}, Table 1, entry 1), the activity of did not show significantly decrease, which excluded the influence of nanoparticle catalysis. Moreover, as revealed in the XPS spectra (Fig. S12), the Ru $3p_{3/2}$ and $3d_{5/2}$ spectra of Ru-CNP complex **1** after CO_2 hydrgogenation reactions at 140 °C and 200 °C didn't show the features of Ru^0,[19] manifesting that the Ru-CNP complex **1** would not be reduced to Ru^0 metal during the reaction, which also ruled out the involvement of nanoparticle catalysis.

Table S4. CO_2 hydrogenation performance of complex **1** in the presence of NaOAc[a].

entry	cat.	Additive	base	TOF (h^{-1})
1	N/A	NaOAc	CsOH	N/A
2	1	NaOAc	N/A	368

3	1	NaOAc	CsOH	1960
4[b]	1	NaOAc	CsOH	1540
5[b]	1	NaOAc	CsOH	1310
6[c]	1	NaOAc	CsOH	1010
7[c]	1	NaOAc	CsOH	1340
8[c]	1	NaOAc	CsOH	2480
9[d]	1	N/A	CsOH	704

[a] General conditions: Complex **1** (0.1μmol), reaction time = 4 h, T = 140 °C, base = CsOH (10 mmol), V(THF)/V(H_2O) = 1:5 (6 ml), H_2 : CO_2 = 2.5:2.5 (MPa), additive (5 mmol); [b] reaction time = 8 h (entry 4), 16 h (entry 5); [c] 1 mmol additive (entry 6), 2 mmol additive(entry 7), 10 mmol additive (entry 8) ;[d] 20 mmol CsOH.

Blank experiment showed that no formate was detected in the absence of ruthenium complex (Table S4, entry1), which proved that NaOAc could not achieve the CO_2 hydrogenation.

The base (10 mmol CsOH) in the system was greatly excessive when NaOAc (2-10 mmol) was added. So if NaOAc merely provided a more basic environment, it shouldn't have such a huge impact on the TOF. To verify our speculation, addition 10 mmol CsOH was added in the system. 20 mmol CsOH could provide a more basic environment than the mixture of 10 mmol CsOH and 10mmol NaOAc (2480 h^{-1}, Table S4, entry 8), because the alkalinity of NaOAc is far less than that of CsOH. The TOF (700 h^{-1}, Table S4, entry 9) in 20 mmol CsOH didn't show obviously enhancement than the original value (700 h^{-1}, Table 1, entry 1), which affirmed that a more basic environment could not ensure a much better activity. According to the relevant literature,[20] it is more likely that OAc^- could coordinate with Ru centers in certain way and play an action as the internal base during the reaction, which then had profoundly influence the catalytic activity.

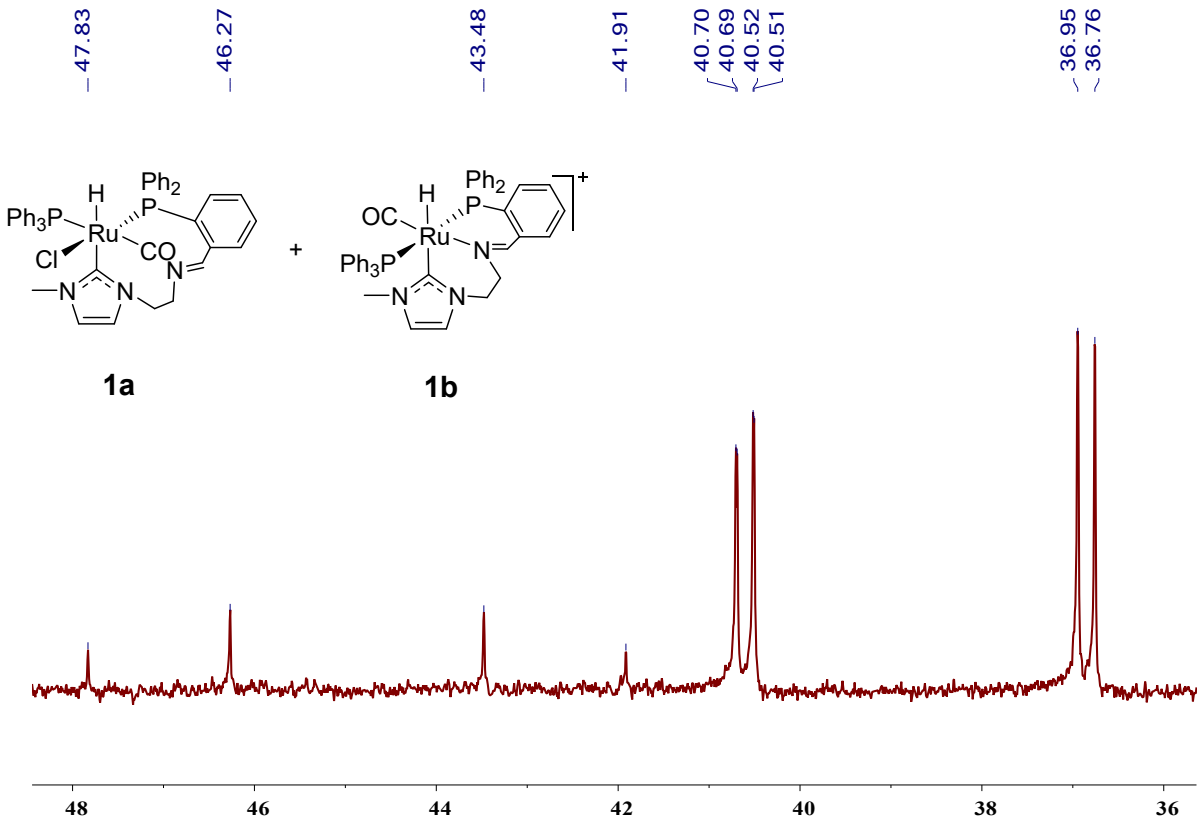

Figure S13. ^{31}P NMR spectrum of pure complex **1a** dissolved in CD_2Cl_2 for 2 h (162.0 MHz, CD_2Cl_2)**.**

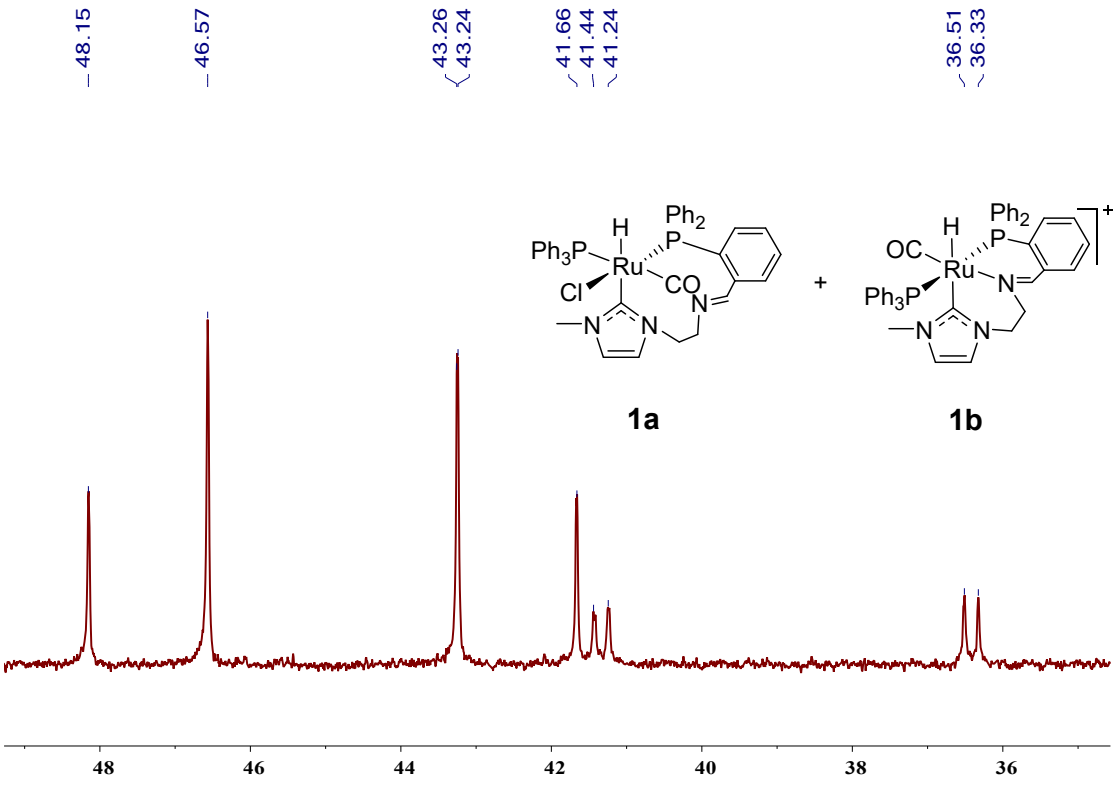

Figure S14. ^{31}P NMR spectrum of pure complex **1b** dissolved in DMSO-d_6 for 2 h (162.0 MHz, DMSO-d_6).

Even though we could obtain pure complex **1b** by column chromatography. There would still be an equilibrium between **1a** and **1b** (Fig. S13-S14) when pure **1a** or pure **1b** was dissolved in the solution **(**CH_2Cl_2 or DMSO-d_6**).**

Therefore, we can't completely rule out complex **1a** as a catalytically competent species. But as revealed by the ^{31}P NMR spectra, most of the complex **1a** transformed to **1b** during the CO_2 hydrogenation reaction (Fig. 2), which suggested that complex **1b** is more likely to be the catalytically competent species.

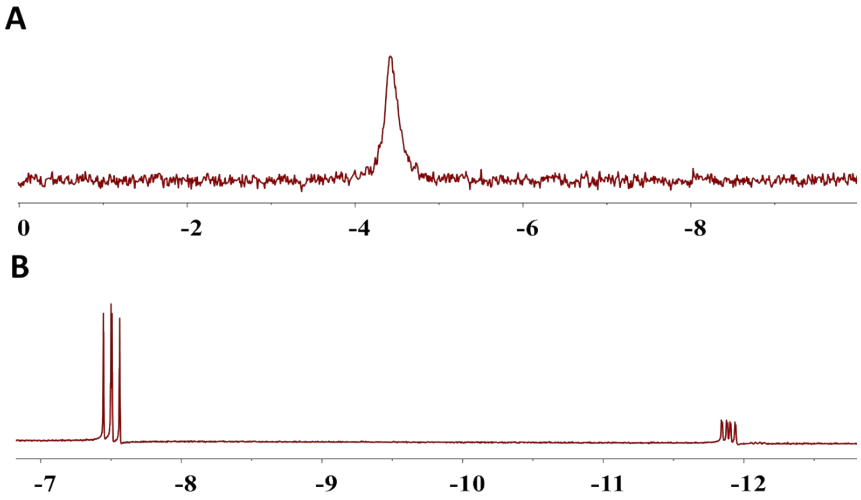

Figure S15. NMR spectra of the reaction mixture: (A) ^{31}P NMR of the free PPh_3; (B) upfield of ^{1}H NMR spectra of the reaction mixture.

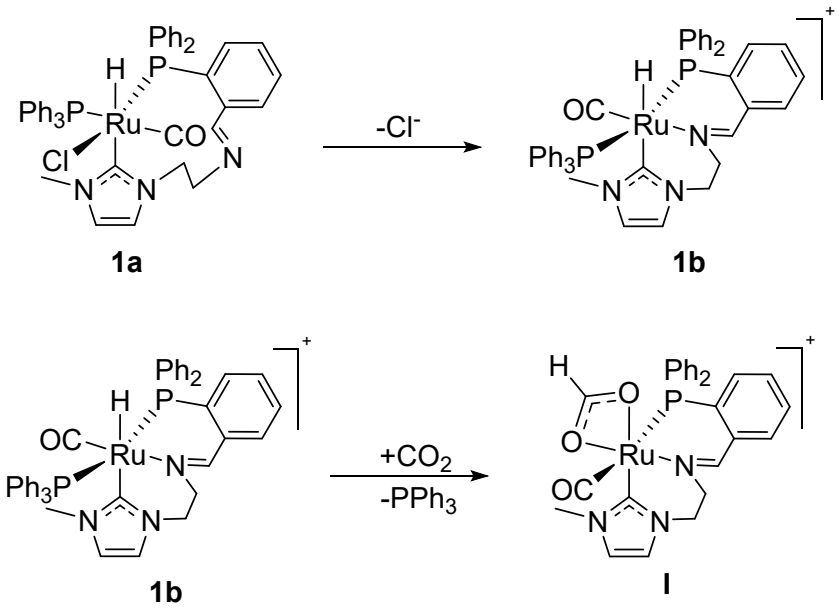

Scheme S6. Summary for the stoichiometric reactions.

In the stoichiometric reactions, ^{31}P NMR spectra displayed that most of the complex **1a** transformed to **1b** during the reaction (Fig. 2A-B). Moreover, the signal of the free

PPh_3 was detected (Fig. S15A), and a signal of the new species appeared at +45 ppm (Fig. 2B), which was not observed without CO_2. At the same time, ^1H NMR spectra showed that the signal located at 8.75 ppm was attributed to $HCOO^-$ (Fig. 2C). So it was reasonable to deduce that the new species was the formate-chelated Ru complex (intermediate **I**), which was formed by the substitution of PPh_3 with $HCOO^-$.

References

1. Y. Li, X. Yu, Y. Wang, H. Fu, X. Zheng, H. Chen and R. Li, *Organometallics*, 2018, **37**, 979-988.
2. X. He, Y. Li, H. Fu, X. Zheng, H. Chen, R. Li and X. Yu, *Organometallics*, 2019, **38**, 1750-1760.
3. R. Tanaka, M. Yamashita and K. Nozaki, *J. Am. Chem. Soc.*, 2009, **131**, 14168-14169.
4. G. A. Filonenko, E. J. Hensen and E. A. Pidko, *Catal. Sci. Technol.*, 2014, **4**, 3474-3485.
5. S. Takaoka, A. Eizawa, S. Kusumoto, K. Nakajima, Y. Nishibayashi and K. Nozaki, *Organometallics*, 2018, **37**, 3001-3009.
6. A. Eizawa, S. Nishimura, K. Arashiba, K. Nakajima and Y. Nishibayashi, *Organometallics*, 2018, **37**, 3086-3092.
7. D. Jantke, L. Pardatscher, M. Drees, M. Cokoja, W. A. Herrmann and F. E. Kühn, *ChemSusChem*, 2016, **9**, 2849-2854.
8. G. A. Filonenko, D. Smykowski, B. M. Szyja, G. Li, J. Szczygieł, E. J. Hensen and E. A. Pidko, *ACS Catal.*, 2015, **5**, 1145-1154.
9. T. T. Thai, B. Therrien and G. S. Fink, *J. Organomet. Chem.*, 2009, **694**, 3973-3981.
10. Z. Dai, Q. Luo, H. Cong, J. Zhang and T. Peng, *New J. Chem.*, 2017, **41**, 3055-3060.
11. M. Scott, B. Blas Molinos, C. Westhues, G. Franciò and W. Leitner, *ChemSusChem*, 2017, **10**, 1085-1093.
12. J. Kothandaraman, M. Czaun, A. Goeppert, R. Haiges, J. P. Jones, R. B. May, G. S. Prakash and G. A. Olah, *ChemSusChem*, 2015, **8**, 1442-1451.
13. C. A. Huff and M. S. Sanford, *ACS Catal.*, 2013, **3**, 2412-2416.
14. S. Sanz, A. Azua and E. Peris, *Dalton Trans.*, 2010, **39**, 6339-6343.
15. A. Weilhard, S. P. Argent and V. Sans, *Nat. Commun.*, 2021, **12**, 231.
16. C. Guan, Y. Pan, E. P. L. Ang, J. Hu, C. Yao, M. H. Huang, H. Li, Z. Lai and K. W. Huang, *Green Chem.*, 2018, **20**, 4201-4205.
17. T. J. Schmeier, G. E. Dobereiner, R. H. Crabtree and N. Hazari, *J. Am. Chem. Soc.*, 2011, **133**, 9274-9277.
18. G. M. Whitesides, M. Hackett, R. L. Brainard, J. P. P. Lavalleye, A. F. Sowinski, A. N. Izumi, S. S. Moore, D. W. Brown and E. M. Staudt, *Organometallics*, 1985, **4**, 1819-1830.
19. D. J. Morgan, *Surf. Interface Anal.*, 2015, **47**, 1072-1079.
20. J. L. Drake, C. M. Manna and J. A. Byers, *Organometallics*, 2013, **32**, 6891-6894.